Nanorod Self-Assembly for Tuning Optical Absorption

Michael J. A. Hore and Russell J. Composto*

Department of Materials Science and Engineering and Laboratory for Research on the Structure of Matter, University of Pennsylvania, Philadelphia, Pennsylvania 19104-6272, United States

ARTICLE

ABSTRACT Metallic nanoparticles that absorb and concentrate light are leading to greater efficiencies in nanophotonic devices. By confining gold nanorods (Au NRs) in a polymer film, we can control their spacing and orientation and, in turn, the absorption and polarization characteristics of the nanocomposite. In this study, we systematically increase the volume fraction of Au NRs (ϕ_{rod}) (aspect ratio $\nu = 3.3$) while maintaining a uniform dispersion. As ϕ_{rod} increases from 1 to 16 vol %, the spacing between rods decreases from 120 to 20 nm and scales as $\phi_{rod}^{-0.4}$. Simultaneously, the local 2D orientational order parameter increases linearly with ϕ_{rod}, although the rods are globally isotropic. The Au NR dispersion is found to depend on the enthalpic interactions between poly(ethylene glycol) brush grafted to the Au NRs and the poly(methyl methacrylate) matrix chains. Furthermore, the plasmon resonance exhibits a red shift with increasing ϕ_{rod}, and coupling is observed for separations up to 70 nm. Because NR spacing and orientation can be finely controlled using polymer matrix, these films are ideally suited for understanding fundamental behavior (*e.g.*, plasmon coupling) as well as practical devices (*e.g.*, solar cells).

KEYWORDS: gold nanorods · polymer nanocomposites · alignment · surface plasmon coupling

Metallic nanoparticles have received widespread attention because they can guide and localize light at the nanometer scale, characteristics that underlie the emerging field of plasmonics. For example, a better understanding of how plasmonic structures trap and enhance light can lead to smaller yet more efficient photovoltaic devices[1] or highly sensitive single-molecule detection.[2] When exposed to light, metallic nanoparticles exhibit collective electron excitations (surface plasmons) that allow them to concentrate and manipulate light in a volume much less than the incident wavelength.[3] The resonance energy for these enhancements depends on the size, shape, and proximity of the nanoscale objects. Pairs of these particles can couple and enhance local electric fields by factors as high as 10^5.[4] The surface plasmons of pairs of adjacent nanoparticles within a distance approximately 2.5 times their size can be coupled, resulting in substantial near-field enhancements that can be exploited in applications such as surface-enhanced Raman spectroscopy (SERS), which is sensitive to single-molecule detection.[4,5]

Currently, advances in using metallic nanoparticles and nanorods (NR) in devices are impeded by a lack of control over their spacing and orientation in thin films. By controlling NR spacing, one can systematically test how plasmonic coupling decays with distance and probe couplings between ensembles of nanoparticles rather than just pairs. In this article, we demonstrate that Au NRs grafted with a poly(ethylene glycol) brush can be dispersed at very high loadings in a polymer matrix without NR aggregation and while maintaining a nearly monodisperse spacing between NR. For the first time, we examine the effect of the matrix/brush interaction, matrix molecular weight, and NR volume fraction on NR dispersion in thin film polymer films and show how the resulting structure (*i.e.*, spacing and orientation of NR) impacts the optical absorption due to surface plasmon resonances. Furthermore, we have obtained results for a monolayer of Au NRs in a polymer matrix, an attractive structure for fabricating SERS substrates and optically active coatings, for example.

Optically, anisotropic metal nanoparticles, such as gold nanorods, are desirable because they can display a large range of accessible surface plasmon resonance wavelengths as compared to nanospheres.[6] Moreover, anisotropic particles exhibit complex ordering behavior that depends on factors such as their concentration and aspect ratio.[7] Additionally, theory[8,9] and experiments[10] have shown that the phase behavior of rod-like particles depends on the

*Address correspondence to composto@seas.upenn.edu.

Received for review July 21, 2010 and accepted October 25, 2010.

Published online November 3, 2010. 10.1021/nn101725j

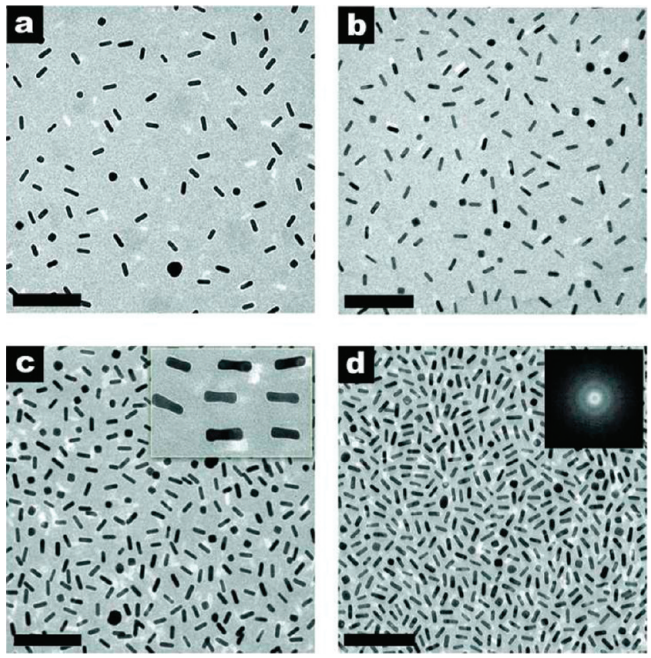

Figure 1. Dispersion and structure of Au NRs in PMMA thin films as a function of volume fraction: (a) $\phi_{rod} = 0.011$, (b) $\phi_{rod} = 0.048$, (c) $\phi_{rod} = 0.095$, (d) $\phi_{rod} = 0.161$. Scale bars are 200 nm. The inset of (c) highlights local alignment and uniform spacing of nanorods. This uniform spacing is also reflected in the Fourier transform of (d) (shown in the inset), which corresponds to a strong correlation at a distance of approximately 29 nm.

dimensionality of the system. For instance, low aspect ratio rods ($\nu < 7$) are unable to order into a nematic phase in two dimensions (2D), whereas in three dimensions (3D), a nematic phase is observed.[8] Instead of a nematic phase in 2D, high concentrations of low aspect ratio rods with $\nu < 7$ exhibit so-called tetratic ordering, characterized by four-fold symmetry between highly ordered grains of rods. Although this tetratic ordering has not yet been observed in polymer nanocomposites, the present article suggests that tetratic ordering may be possible in polymer nanocomposite films. More recently, Wilson *et al.*[11] have shown that the presence of an adsorbing polymer chain on a nanoparticle can affect the phase behavior of nanorods. In particular, the assembly of NRs into a nematic phase can be enhanced or suppressed by simply varying the tethered chain length, indicating that the ordering behavior of nanorods in polymer nanocomposites does not necessarily obey classical theories such as those of Onsager.[7] Yockell-Lelievre *et al.*[12] explored the effect of polymer brushes on the morphology of nanoparticle arrays. By casting polystyrene (PS)-functionalized nanoparticles from chloroform onto a surface, large 2D arrays of particles were assembled whose interparticle spacing depended on the length of the PS brush.

Perez-Juste *et al.*[13] demonstrated that Au NRs can be aligned by applying a mechanical stress to a poly(vinyl alcohol) film. This device was observed to selectively absorb polarized light at wavelengths that can be tuned by varying the aspect ratio of the nanorods.[13] Hu *et al.* have shown[14] that CdSe and CdTe nanorods can be aligned by applying an external electric field. In addition, Mohraz and Solomon[15] investigated the orientation of micrometer-scale poly(methyl methacrylate) (PMMA) particles and found that self-assembled rods of moderate aspect ratio, ν from 5.2 to 12.8, can align at sufficiently high loadings, in qualitative agreement with classical work by Onsager.[7] Deshmukh and co-workers[16] confined Au NRs in a poly(styrene-*b*-methyl methacrylate) block copolymer and achieved substantial lateral alignment of the particles, demonstrating that block copolymers can guide the alignment of nanoparticles. Furthermore, Liu and co-workers[17] recently demonstrated the potential for the fabrication of thermochromic devices through controlled reshaping of Au NRs in PMMA thin films. Nie *et al.*[18] studied absorption spectra of chains of nanorods, further demonstrating the importance of the interplay between nanoparticle size and arrangement in determining optical properties of assemblies. By combining controlled reshaping with an understanding of nanorod alignment in polymer nanocomposites, very precise control of the optical and electrical properties of nanocomposites can lead to new applications such as in optically active sensors or coatings.

RESULTS AND DISCUSSION

Representative TEM images for the PMMA films of thickness $h = 30$ nm containing Au NR volume fractions ϕ_{rod} = (a) 0.011, (b) 0.048, (c) 0.095, and (d) 0.161 are shown in Figure 1. The Au NRs have an average radius of $r_{rod} = 7$ nm and an average length of $l_{rod} = 47$ nm. Note that, even at high NR loadings, the particles remain well-dispersed and the distance between rods is quite regular. This superb dispersion may be attributed to the favorable wetting between the PEG brush and the PMMA matrix which provides an energetic penalty for nanorods to be in contact, resulting in very uniform spacing between NRs. The average distances between neighboring nanoparticles (r_{avg}) are approximately 120, 70, 50, and 30 nm, respectively. These distances are on the order of, or less than, the separations necessary to observe surface plasmon coupling, namely, less than ~120 nm. Qualitatively, at each ϕ_{rod}, neighboring nanorods are observed to align parallel to each other (inset of Figure 1c).

To quantify the ordering in these films, the 2D orientational order parameter S_{2D} was calculated from transmission electron microscopy (TEM) images as

$$S_{2D}(r) = \frac{1}{N_{rod}} \sum_{i=1}^{N_{rod}} \cos 2\theta_i$$

where θ_i is the angle between nanorod i and the nematic director (*i.e.*, average orientation of Au NRs) in a region of size r around the nanorod, and N_{rod} is the number of Au NRs in that region. This is illustrated in

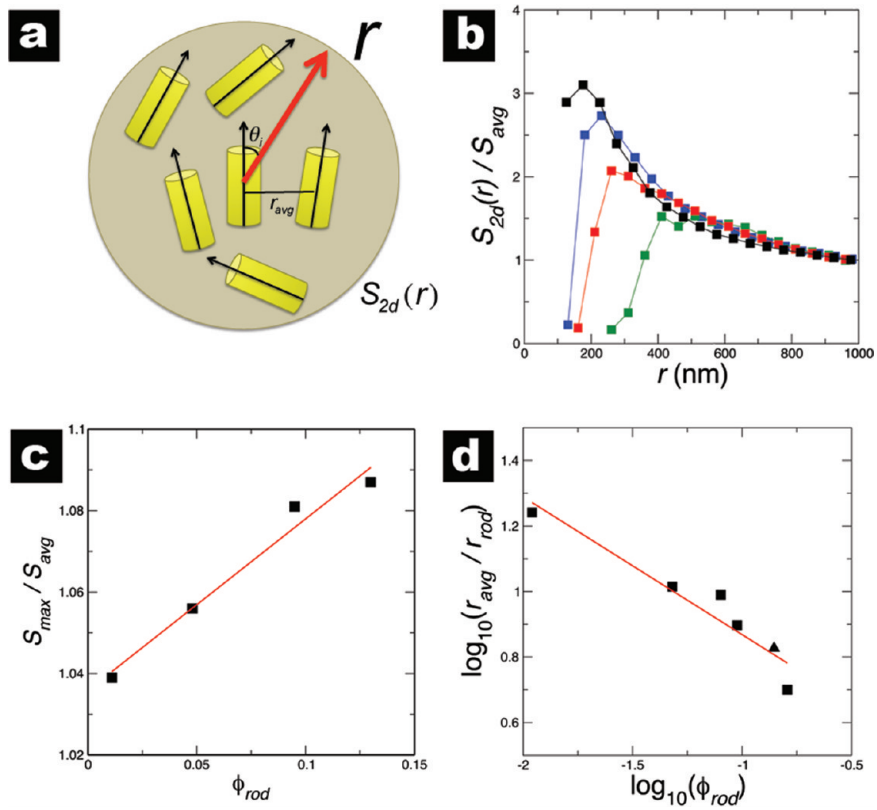

Figure 2. Quantitative analysis of Au NR ordering and dispersion in PMMA thin films. (a) Illustration of the 2D order parameter S_{2D}, which quantifies the degree of ordering in a region of size r. S_{2D} ranges from 0 for isotropic configurations to 1 for perfectly aligned rods. (b) Two-dimensional orientation order parameter normalized by S_{avg} plotted as a function of distance for $\phi_{rod} = 0.011$, 0.048, 0.095, and 0.161 (bottom to top). (c) Maximum value of $S_{2D}(r)$ normalized by S_{avg} plotted as a function of nanorod volume fraction. (d) Average inter-rod spacing divided by rod radius plotted as a function of concentration on a double logarithmic scale. The dashed line has a slope of −0.4. From a geometrical argument, the rod spacing should decay as $\phi_{rod}^{-0.5}$; however, experiments show a weaker dependence of $r_{avg} \sim \phi_{rod}^{-0.4}$.

Figure 2a, where the nematic director is schematically represented by the red arrow. We define the average global order, $S_{avg} = S_{2D}(r)$, when r is the lateral size of the TEM micrograph (approximately 1 μm). As the volume fraction of nanorods increases, NR ordering in the films increases strongly. This is substantiated in Figure 2b, where S_{2D}/S_{avg} is plotted as a function of distance, r, for the systems shown in Figure 1. The Au NR volume fractions are $\phi_{rod} = 0.011$, 0.048, 0.095, and 0.161 from bottom to top at $r = 300$ nm. The data are normalized by the global order parameter S_{avg}. For each value of ϕ_{rod}, Figure 2b shows that NR ordering increases, reaches a maximum value S_{max}/S_{avg}, and then slowly decreases toward 1 over a distance of 1000 nm (~20 L_r) as r increases. The initial increase reflects the lower density of rods in the immediate vicinity of a central rod due to the excellent dispersion of nanoparticles (*i.e.*, only PMMA around the rods). After the initial increase, high local ordering is maintained over distances of several hundred nanometers. Finally, over large distances ($r >$ 500 nm), the order parameter decays in a manner that is invariant with respect to the nanoparticle concentration to a value of $S_{2D} \approx 0.1$. This behavior is in quantitative agreement with theory[8,9] which predicts that rods with low aspect ratios ($\nu < 7$) are globally isotropic at large distances. Because of the limited size of the TEM image (~1 μm^2), the number of NRs (N_{rod}) is insufficient to yield $S_{avg} = 0$. Nevertheless, the experimental S_{avg} values for $r = 1000$ nm are small ($S_{avg} = 0.18 \pm 0.05$), suggesting that these films are isotropic at long distances. Figure 2c shows that the normalized maximum ordering increases linearly with ϕ_{rod}. The values of S_{max} increase from 0.1 to 0.5 as ϕ_{rod} increases from 0.011 to 0.161. Additional theory is necessary to understand why local order increases linearly with ϕ_{rod}.

A striking feature of the TEM micrographs (Figure 1) is that the Au NRs maintain very uniform interparticle separations, especially noticeable at higher concentrations. Figure 2d shows that the average inter-rod spacing, r_{avg}, plotted on a double logarithmic scale decreases monotonically as ϕ_{rod} increases. For comparison, consider a system of nanorods that are homogeneously dispersed at low volume fractions (*e.g.*, $\phi_{rod} = 0.011$). As volume fraction increases (*i.e.*, rods added), new rods uniformly fill the gaps between previously placed rods. For such noninteracting NRs in 2D, the inter-rod distance scales as $\phi_{rod}^{-0.5}$. A fit to our data (Figure 2d) yields a similar dependence $r_{avg} \sim \phi_{rod}^{-0.4}$, indicating that the nanorods are packing in a 2D manner. Preliminary X-ray reflectivity measurements (not

shown) also indicate that the nanorods are not uniformly distributed throughout the film but are confined to a region near the substrate approximately $2r_{rod}$ thick. The small difference between the experimental dependence of r_{avg} on the volume fraction and the ideal dependence may be attributed to the presence of approximately 10% nanospheres that frustrate rod packing relative to that of a pure rod system and/or interactions between the PEG brush and PMMA that push rods away from each other.

For rods confined in 2D, the overlap volume fraction at which the pervaded volumes of nanorods in the nanocomposite film begin to overlap, ϕ^*, is given by

$$\phi^* = \left(\frac{r_{rod}}{h}\right)\frac{1}{\nu} \approx \frac{4.17}{h}$$

where ν is the NR aspect ratio ($l_{rod}/2r_{rod}$) and h is the film thickness. Thus, for a given r_{rod}, ϕ^* decreases as ν increases. For $h = 30$ nm and $\nu = 3.3$, $\phi^* \approx 0.14$. Using simple geometry, at $\phi_{rod} = \phi^*$, the inter-rod spacing is equal to l_{rod} (47 nm), as denoted by the triangular point in Figure 2d. The agreement between our data and these estimations further implies that the nanorods may be behaving as 2D objects.

The inter-rod spacing and NR ordering may also depend on the molecular weight of the matrix polymer. In addition to the PMMA (82.4 kg/mol) matrix used earlier (*e.g.*, Figure 1), PMMA (38.5 kg/mol) and PMMA (320 kg/mol) were also investigated to determine if an increase in the radius of gyration, R_g, from 5.4 to 15.9 nm (*i.e.*, $\sim 1-2r_{rod}$), could increase the inter-rod spacing. Representative TEM images for the low and high molecular weight systems at the same ϕ_{rod} (=0.080) are shown in Figure 3a,b, respectively. Figure 3c (bottom right) shows the orientational correlation function $g_2(r)$ for the 38.5 and 320 kg/mol PMMA matrices, along with the simulation (black squares) for noninteracting nanorods of the same aspect ratio and volume fraction. The angular correlation function represents the degree of orientational correlations between a central NR and those located a distance r away and is defined as

$$g_2(r) = \langle \cos 2[\theta_i(0) - \theta_j(r)] \rangle$$

where $\theta_i(0) - \theta_j(r)$ is the difference in the orientational angles between a rod at the origin and those a distance r away. The angular correlation function is illustrated in Figure 3c (top right). For reference, parallel and perpendicular rods have $g_2 = 1$ and $g_2 = -1$, respectively. For an isotropic system, the average value of g_2 is given by the orientational average of g_2 and is therefore 0.

Figure 3c (bottom right) shows that the orientational correlations decay over a distance that is independent of the matrix molecular weight. For both the

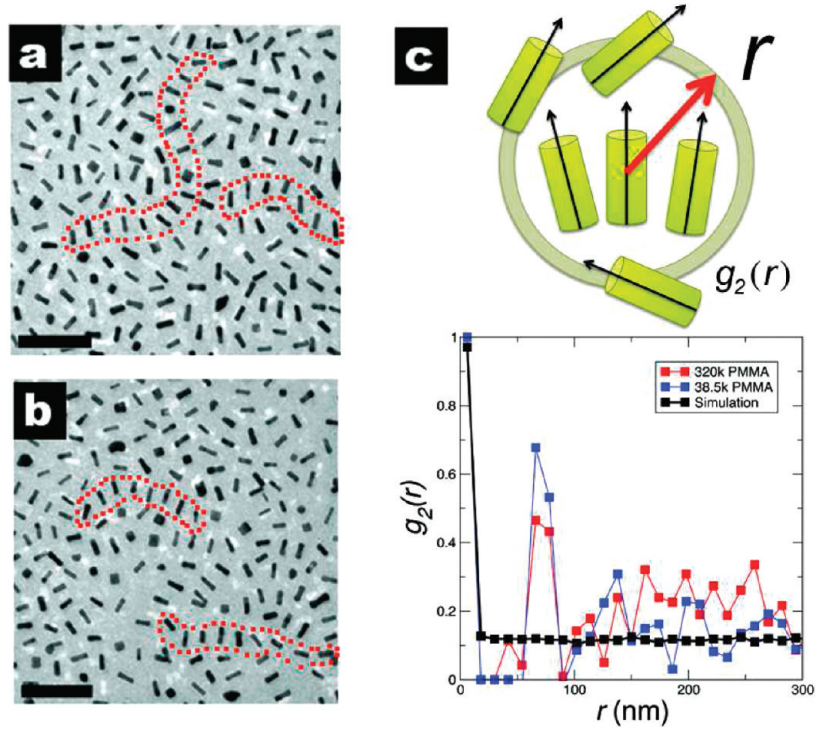

Figure 3. Analysis of molecular weight dependence. Representative TEM images of Au NRs at $\phi_{rod} = 0.080$ in PMMA matrices having molecular weights of (a) 38.5 kg/mol and (b) 320 kg/mol. Dotted lines show correlations between side-by-side neighbors. Scale bars are 200 nm. (c) Orientational correlation functions g_2 for the films in (a) and (b); g_2 quantifies the degree to which a nanorod at the origin is correlated with those a distance r away and takes values of 1 for perfectly correlated rods and 0 for uncorrelated rods. For $\phi_{rod} = 0.080$, the order correlation function is plotted as a function of distance for the low (a) and high (b) molecular weight PMMAs, as well the noninteracting NR simulation. For the experimental system, the high secondary peaks in g_2 (0.7 and 0.5) denote strong correlations between nearest-neighbor nanorods up to distances of $\sim$70 nm.

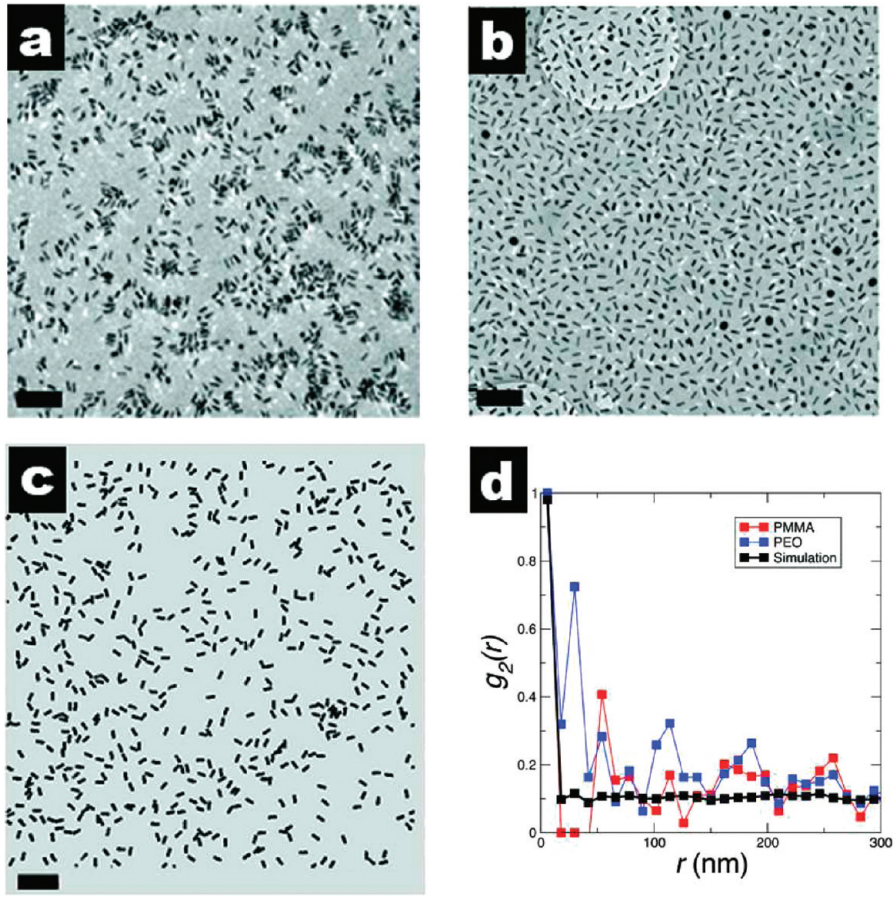

Figure 4. Effect of matrix type on NR dispersion and correlation. (a) Representative TEM image of NRs at $\phi_{rod} = 0.038$ in a PEO matrix. Because enthalpic interaction is weak, the NRs are attracted by depletion−attraction forces resulting in aggregation. (b) NRs at $\phi_{rod} = 0.048$ in a PMMA matrix. Nanorods interact favorably with the matrix chains in this case promoting good dispersion. (c) Simulation snapshot for noninteracting rods at $\phi_{rod} = 0.038$. Scale bars are 200 nm. (d) Order correlation function plotted as a function of distance for systems in (a−c). Nanorods in the PEO matrix exhibit short-range correlations in orientation due to their aggregation, whereas nanorods in PMMA exhibit longer-range correlations over distances of 50 nm. The nanorods in the simulation are uncorrelated.

low (38.5 kg/mol) and high (320 kg/mol) molecular weight matrices, the nanorods become uncorrelated beyond 70 nm, corresponding to distances after the secondary peak in g_2. For the noninteracting rod simulation, g_2 decreases sharply near $r = 0$ and no secondary peak is observed, indicating that the orientations for the nanorods are uncorrelated. For TEM images, such as Figure 3a,b, the average inter-rod spacing is found at a distance of $r_{avg} \approx 69$ nm (*e.g.*, Figure 3a,b), indicating that the secondary peaks of $g_2(r)$ in Figure 3c correspond to correlations between nearest neighbors. Thus, as noted previously for PMMA (82.4 kg/mol), NRs are highly correlated with their nearest neighbors at all molecular weights investigated. Futhermore, this correlation can propagate throughout the film and gives rise to the high ordering observed at intermediate (hundreds of nanometers) length scales, as shown in Figure 2b. The dotted lines in Figure 3a,b denote correlations consisting of side-by-side chains of nanorods. The observation of a correlation between neighboring nanorod orientations over such large distances is informative. For example, these correlations persist well beyond a rod length $l_{rod} = 47$ nm, which suggests that the matrix chains between rods play a role in promoting order. It is important to note, however, long-range order across the film is not observed—a result in agreement with theoretical predictions[8,9] and previous observations.

For the systems presented thus far, the nanorods have a favorable interaction with the polymer matrix that promotes their dispersion. To understand the role of the NR−matrix interaction on ordering, the same PEG-modified Au NRs are incorporated into a poly(ethylene oxide) (PEO) matrix. PEO has an identical repeat unit (CH_2CH_2O) as the PEG brush and therefore provides a neutral environment for the PEG-modified NRs. Under these conditions, the brush/matrix interaction should be predominantly entropic. For NRs at $\phi_{rod} = 0.038$ in a PEO matrix, the PEG-functionalized Au NRs form small aggregates which are separated by large regions of PEO, as shown in Figure 4a. This aggregation can be attributed to a depletion−attraction interaction between NRs, predicted theoretically using density functional theory simulations by Frishknecht.[19] The

depletion−attraction interaction is caused by a gain in entropy of matrix chains upon displacing them from between particles (*i.e.*, confinement) to the bulk. Note that the nanorods within each aggregate do not come into core−core contact because the PEG brush provides a repulsive interaction at close separations. Although their size varies, the typical aggregate is about 200 nm. Because of the close proximity of neighboring rods in aggregates and large spacing between aggregates, orientational order should be high near the rod and quickly decay beyond the aggregate size.

To gain insight into the PEO case, a noninteracting rod simulation was performed at the same ϕ_{rod}. In contrast to the uniform dispersion in the PMMA matrix, the NRs in PEO and the simulation show a much wider range of separation, an observation shared by recent work by Akcora *et al.*[20] for polystyrene-grafted silica nanospheres in polystyrene thin films. The similarity and difference between NR assembly in the PEO film and the simulation can be seen by comparing Figure 4a,c. Similar to the PEO case (Figure 4a), large regions of the simulation space are devoid of NRs, as shown in Figure 4c. However, the aggregates are more diffuse because NRs are not as closely packed as in the PEO case (Figure 4a). Both Figure 4a and Figure 4c are in stark contrast with Figure 4b, where excellent dispersion of NRs in PMMA is observed over large length scales. Figure 4d shows the order parameter correlation functions for Au NRs in PMMA ($\phi_{rod} = 0.048$) and PEO ($\phi_{rod} = 0.038$), as well as the noninteracting rod simulation ($\phi_{rod} = 0.038$). Similar to the results in Figure 3c, secondary peaks that correspond to nearest-neighbor correlations in orientation are observed in the experimental systems but absent in the simulation. From Figure 4d, the nanorods in the simulation become uncorrelated after approximately 18 nm, whereas the nanorods in the PEO matrix maintain correlations in their orientation up to a distance of about 31 nm. Interestingly, nanorods maintain their orientational correlations in the PMMA matrix at longer distances (>50 nm) despite having nearly the same volume fraction. Upon comparing the order correlation functions of NRs in PMMA at $\phi_{rod} = 0.080$ (Figure 3a,b) and $\phi_{rod} = 0.048$ (Figure 4d), the secondary peak position decreases from 70 to 50 nm, respectively. This observation is consistent with the behavior of the 2D order parameter (Figure 2b), which shows that local ordering increases and is longer range as ϕ_{rod} increases. The different behavior of g_2 in the simulation and the PEO matrix case can be explained by noting that the NRs in the PEO matrix are attracted to each other by depletion−attraction forces but prevented from touching each other by the PEG brushes. This leads to short-range order correlations in the PEO matrix that are absent in the simulation.

The favorable interaction between the PEG brush and PMMA matrix plays a prominent role in the orientational correlations between rods. When Au NRs are incorporated into a PEO matrix that is chemically identical to the PEG brush, the nanorod spacing decreases to a value independent of ϕ_{rod} and nanorods form clusters which are on the order of 200 nm in size. In the PEO matrix, local orientational correlations between neighboring NRs are observed, although these correlations rapidly decay because of the large spacing between aggregates. These observations suggest that NR phase separation in PEO is entropically driven—a result in agreement with simulations by Frishknecht[19] and experimental observations by Akcora *et al.*[20]

Controlling the spacing and orientation of nanorods is a significant step toward enhancing their use in applications, such as surface-enhanced Ramen spectroscopy, that utilize coupling of surface plasmons. Both theory and experiments[2,4−6] show that nanorods in close proximity can affect the wavelengths that excite surface plasmons. Furthermore, the magnitude of this shift and direction (*i.e.*, blue shift or red shift) is very sensitive to the orientation of neighboring nanorods with respect to each other. Figure 5a shows the UV/vis spectra for Au NRs in H_2O and PMMA thin films ($h \approx 30$ nm) at $\phi_{rod} = 0.011$, 0.048, and 0.095. Figure 5b shows that an increase in nanorod concentration leads to a red shift in the position of the longitudinal surface plasmon resonance (LSPR), compared to single rods in solution. The offset (~0.018) at $\phi_{rod} = 0.011$ is due to increasing the refractive index of the matrix from water to PMMA. The subsequent increase in ϕ_{rod} results in a monotonic increase in the LSPR, corresponding to a red shift $\Delta\lambda$ with respect to the initial LSPR wavelength λ_0. This behavior is in good qualitative agreement with recent work by Funston *et al.*,[5] where red shifts in the LSPR were observed for pairs of nanorods with different orientations on indium tin oxide (ITO)-coated glass in air. In our experimental studies, as the concentration of nanorods increases (*i.e.*, inter-rod spacing decreases), the red shift of the LSPR position can be as large as 50 nm. We note that the magnitude of this red shift is larger than those reported by Funston *et al.*[5] because our experiments are probing an ensemble of nanorods rather than individual pairs. Indeed, shifts as large as 200 nm have been seen by Nie *et al.*[18] for long, isolated chains of nanorods. It also is worth noting that the shift in Figure 5b is not solely due to nanorod−nanorod coupling but also scattering within the film and higher order couplings between nanorods that, to our knowledge, have not yet been modeled. The inset of Figure 5b shows a fit of the percent shift of the LSPR position predicted by the Universal Plasmon Ruler model,[5,21,22] $\Delta\lambda/\lambda_0 \sim \exp(-r_{avg}/2\tau r_{rod})$, where τ is a prefactor defining the range of the plasmon coupling. Our fit yields $\tau = 6.6$, indicating that NRs separated by 100 nm (*i.e.*, twice the NR length) or less exhibit coupling. Independent of nanoparticle shape for dimers and trimers of particles, Jain and El-Sayed found that $\tau = 0.2$ but noted that

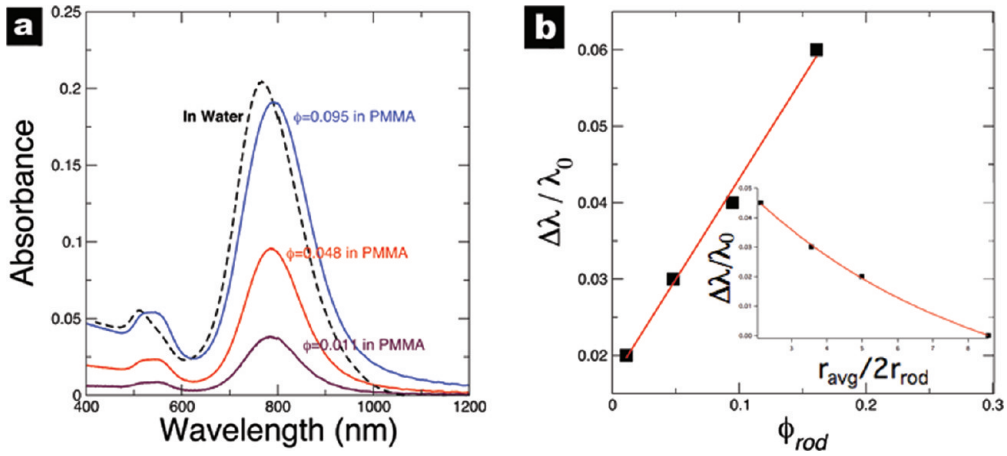

Figure 5. (a) UV/vis spectra for Au NRs in water (dashed line) and PMMA films (solid lines) for ϕ_{rod} = 0.011, 0.048, and 0.095. (b) Percent red shift in the longitudinal surface plasmon resonance (LSPR) wavelength as a function of NR volume fraction. The line is a least-squares fit $\Delta\lambda/\lambda_0 = 0.231\phi_{rod} + 0.018$, where λ_0 is the position of the LSPR for the NRs in water. The initial shift at ϕ_{rod} = 0.011 is due from changing the medium from water to PMMA. The increase in red shift results from a decrease in NR spacing with an increase in ϕ_{rod}, as noted in Figure 2d. The inset shows a fit of the LSPR shift (relative to ϕ_{rod} = 0.011) to the Universal Plasmon Ruler model.

electromagnetic retardation and other effects are important for large arrays of nanoparticles and could change the prefactors.[22] Nevertheless, because their optical properties are tunable and predictable (*e.g.*, Figure 5), nanocomposite films of Au NRs in PMMA have potential applications as polarization-dependent absorption filters, thermochromic sensors, and strain gauges.

CONCLUSION

In summary, we have explored the local ordering of Au NRs in two distinct polymer film systems. In the first, Au NRs that are functionalized with a PEG brush are incorporated into PMMA films with a thickness of $h = 30$ nm that confines the NRs to lie in the plane of the film. Because the PEG brush has a favorable interaction with PMMA, the NRs are well-dispersed in the PMMA matrix and exhibit a nearly uniform inter-rod spacing. This spacing is found to decrease with increasing nanorod concentration, whereas local orientational order increases. Although the local ordering of NRs decays over hundreds of nanometers, the NRs are isotropic at large length scales (*i.e.*, no global ordering). The optical properties of the NR/PMMA nanocomposites vary in a systematic fashion, which makes these films attractive as coatings (*e.g.*, filters) or other sensing devices. In the second nanocomposite system, the PMMA matrix was replaced by a PEO matrix that is chemically identical to the PEG brush on the NRs. In this case, because the enthalpic interaction between the NRs and the matrix is negligible, poor dispersion of the particles is seen due to the conformation entropy cost of matrix chains located between nanorods, namely, depletion−attraction forces.

The present advancement in nanorod composite films raises interesting directions for future studies. For example, grazing incidence small-angle X-ray scattering (GISAXS) can be used to support our observation of long-range order of the nanorods and extend the length scale of the measurement beyond that accessible by TEM. In addition, by incorporating a deuterated tracer into the PMMA or PEO matrix, small-angle neutron scattering (SANS) can be used to determine the effect of nanorods on the radius of gyration of the matrix chains confined between NRs. These studies would provide insight into the role of interactions between the PEG brush and matrix chains on the orientation correlations between neighboring nanorods. From a theoretical standpoint, simulations of the inter-rod potential that incorporate enthalpic interactions between the nanorods and the matrix are needed. These simulations would provide guidelines for predicting NR aggregation as well as changes in the conformation of matrix chains adjacent to the NRs. For instance, density functional theory simulations performed by Frishknecht[19] modeled forces between NRs that have a brush which is identical to the polymer matrix. If the brush is the same size or larger than the matrix chains, NRs are predicted to disperse. However, if the brush is shorter than the matrix chains, depletion−attraction forces are expected to produce aggregation. By incorporating an attractive force between the matrix and the brush, the effect of matrix molecular weight and composition on inter-rod forces could be addressed. Furthermore, these simulations can provide insight into the mechanism for local ordering of the Au NRs in the PMMA matrix. With these questions addressed in homopolymer matrices, studies of NR ordering in block copolymer matrices could be designed in a targeted manner, allowing for finer control over the long-range order of NRs, with the eventual goal of creating advanced optical devices. For example, a poly(styrene-*b*-methyl methacrylate) co-

polymer film can achieve long-range order by applying shear flow[23] or electric fields.[24,25] By incorporating NRs into the PMMA domains (lamellae or cylinders), fine control over nanorod orientation could be realized (*e.g.*, 2D or 1D orientation) and incorporated into future devices.

METHODS

To study the ordering of Au NRs in polymer thin films, we incorporated poly(ethylene glycol) (PEG)-functionalized Au NRs into both PMMA and poly(ethylene oxide) thin films. The matrix polymers poly(methyl methacrylate) (PMMA, M_w = 38.5, 82.4, 320 kg/mol) and poly(ethylene oxide) (PEO, M_w = 102 kg/mol) were purchased from Polymer Source, Inc. (Montréal, Canada) and used as received. Reagants used in the synthesis of the nanorods were purchased from Sigma Aldrich and used as received. Water was obtained from a Millipore water purification system. Au NRs were synthesized following a seeded growth method.[26,27] Briefly, 1.7 mL of 0.1 M $HAuCl_4 \cdot 3H_2O$, 250 μL of $AgNO_3$, 270 μL of ascorbic acid, and 420 μL of a gold seed solution were added to 45 mL of 0.1 M hexadecyltrimethylammonium bromide (CTAB) and incubated at 33 °C for a minimum of 3 h. The concentrations were chosen to maximize nanorod yield and resulted in nanorods with an average radius of r_{rod} = 7 nm and length l_{rod} = 47 nm. After centrifuging twice to remove excess CTAB from the solution, 10 mL of a concentrated NR solution was combined with 8 mL of a 1 mM solution of thiol-terminated poly(ethylene glycol) (PEG, M_w = 5 kg/mol) and shaken for 2 h.[28] Rods were then transferred to methanol by centrifuging the concentrated solution at 8000 rpm for 20 min and discarding the supernatant. This method was repeated to transfer the rods into toluene. Thin films were prepared by spin coating from a 1 wt % polymer/nanorod and toluene solution onto clean silicon or glass substrates at 2000 rpm for 60 s. Films were then dried for 24 h in a fume hood. The resulting films had thicknesses of 30 ± 1 nm determined by ellipsometry and Rutherford backscattering spectrometry (RBS).

Ordering of Au NRs in PMMA thin films was investigated by transmission electron microscopy (TEM) on a JEOL JEM 2010 at 80 kV. The lower voltage of 80 kV was chosen to minimize degradation of the polymer matrix under the electron beam. Specimens were prepared by floating the films from the silicon substrates onto a water bath and picking the films up on holey carbon TEM grids (Structure Probe, Inc.). TEM micrographs were processed in ImageJ using a collection of plugins[29] from which an orientation vector for each rod could be constructed. From the nanorod orientation vectors, the 2D orientational order parameter S_{2D} and angular correlation functions g_2 were calculated.[8,9] By normalizing S_{2D} by S_{avg}, the variations in S_{2D} due to different sampling statistics at low and high ϕ_{rod} (*i.e.*, N_{rod} is smaller at low ϕ_{rod}) are accounted for.

To further characterize the NRs, the average rod−rod spacing, r_{avg}, was determined and measured relative to the average center of nanorods from TEM images. For each rod, the average nearest-neighbor distance was calculated and averaged across 10 separate micrographs for each system to eliminate statistical deviations.

To compare experimental results to ideal conditions where rods are monodisperse and noninteracting, we performed simulations and calculated the quantities S_{2D}, g_2, and r_{avg}. The simulation was performed by randomly inserting "hard-core" rods into a monolayer. If an inserted rod overlapped with an existing one, the rod was removed and inserted into another random position. The results of 10 independent simulations were then averaged to determine S_{2D}, g_2, and r_{avg}.

Optical properties of the nanorods in solution and polymer films were measured using UV−visible spectroscopy (UV/vis, Varian, Cary 5000 UV/vis spectrophotometer). The initial concentrations of nanorods in the films were determined through a combination of RBS (NEC Corporation 5 SDH Pelletron) and UV/vis. Peak intensity of the longitudinal surface plasmon resonance (LSPR), α_{max}, is linearly proportional to the gold volume fraction ϕ_{rod} determined by RBS. A fit to these data provides a relationship between the volume fraction and the magnitude of the absorbance $\phi_{rod} = 0.514\alpha_{max} - 0.003$, where α_{max} is the peak intensity of the absorbance due to the excitation of longitudinal surface plasmons. Using this relationship, the Au NR volume fraction can be determined rapidly from routine UV/vis measurements rather than the time-consuming RBS technique.

Acknowledgment. This work was supported by the National Science Foundation with primary support from the Polymer (DMR09-07493), MRSEC (DMR05-20020), and IGERT (DGE-0221664) Programs. Secondary support was provided by NSF/NSEC (DMR08-32802). We gratefully acknowledge the assistance and guidance of Y. Liu in the preparation of Au NRs and TEM specimens.

REFERENCES AND NOTES

1. Kelzenberg, M. D.; Boettcher, S. W.; Petykiewicz, J. A.; Turner-Evans, D. B.; Putnam, M. C.; Warren, E. L.; Spurgeon, J. M.; Briggs, R. M.; Lewis, N. S.; Atwater, H. A. Enhanced Absorption and Carrier Collection in Si Wire Arrays for Photovoltaic Applications. *Nat. Mater.* **2010**, *9*, 239–244.
2. Aizpurua, J.; Bryant, G. W.; Richter, L. J.; García de Abajo, F. J. Optical Properties of Coupled Metallic Nanorods for Field-Enhanced Spectroscopy. *Phys. Rev. B* **2005**, *71*, 235420.
3. Schuller, J. A.; Barnard, E. S.; Cai, W.; Jun, Y. C.; White, J. S.; Brongersma, M. L. Plasmonics for Extreme Light Concentration and Manipulation. *Nat. Mater.* **2010**, *9*, 193–204.
4. Jain, P. K.; El-Sayed, M. A. Plasmonic Coupling in Noble Metal Nanostructures. *Chem. Phys. Lett.* **2010**, *487*, 153–164.
5. Funston, A. M.; Novo, C.; Davis, T. J.; Mulvaney, P. Plasmon Coupling of Gold Nanorods at Short Distances and in Different Geometries. *Nano Lett.* **2009**, *9*, 1651–1658.
6. Link, S.; El-Sayed, M. A. Spectral Properties and Relaxation Dynamics of Surface Plasmon Electronic Oscillations in Gold and Silver Nanodots and Nanorods. *J. Phys. Chem. B* **1999**, *103*, 8410–8426.
7. Onsager, L. The Effects of Shape on the Interaction of Colloidal Particles. *Ann. N.Y. Acad. Sci.* **1949**, *51*, 627–659.
8. Bates, M. A.; Frenkel, D. Phase Behavior of Two-Dimensional Hard Rod Fluids. *J. Chem. Phys.* **2000**, *112*, 10034–10041.
9. Triplett, D. A.; Fichthorn, K. A. Monte Carlo Simulation of Two-Dimensional Hard Rectangles: Confinement Effects. *Phys. Rev. E* **2008**, *77*, 011707.
10. Narayan, V.; Menon, N.; Ramaswamy, S. Nonequilibrium Steady States in a Vibrated-Rod Monolayer: Tetratic, Nematic, and Smectic Correlations. *J. Stat. Mech.* **2006**, P01005.
11. Wilson, M. R.; Thomas, A. B.; Dennison, M.; Masters, A. J. Computer Simulations and Theory of Polymer Tethered Nanorods: The Role of Flexible Chains in Influencing Mesophase Stability. *Soft Matter* **2009**, *5*, 363–368.
12. Yockell-Lelievre, H.; Desbiens, J.; Ritcey, A. M. Two-Dimensional Self-Organization of Polystyrene-Capped Gold Nanoparticles. *Langmuir* **2007**, *23*, 2843–2850.
13. Perez-Juste, J.; Rodriguez-Gonzalez, B.; Mulvaney, P.; Liz-Marzan, L. M. Optical Control and Patterning of Gold-Nanorod-Poly(vinyl alcohol) Nanocomposite Films. *Adv. Funct. Mater.* **2005**, *15*, 1065–1071.
14. Hu, Z.; Fischbein, M. D.; Querner, C.; Drndic, M. Electric-Field-Driven Accumulation and Alignment of CdSe and CdTe Nanorods in Nanoscale Devices. *Nano Lett.* **2006**, *6*, 2585–2591.
15. Mohraz, A.; Solomon, M. J. Direct Visualization of Colloidal Rod Assembly by Confocal Microscopy. *Langmuir* **2005**, *21*, 5298–5306.

16. Deshmukh, R. D.; Liu, Y.; Composto, R. J. Two-Dimensional Confinement of Nanorods in Block Copolymer Domains. *Nano Lett.* **2007**, *7*, 3662–3668.
17. Liu, Y.; Mills, E. N.; Composto, R. J. Tuning Optical Properties of Gold Nanorods in Polymer Films through Thermal Reshaping. *J. Mater. Chem.* **2009**, *19*, 2704–2709.
18. Nie, Z.; Fava, D.; Kumacheva, E.; Zou, S.; Walker, G. C.; Rubinstein, M. Self-Assembly of Metal-Polymer Analogues of Amphiphilic Triblock Copolymers. *Nat. Mater.* **2007**, *6*, 609–614.
19. Frishknecht, A. L. Forces between Nanorods with End-Adsorbed Chains in a Homopolymer Melt. *J. Chem. Phys.* **2008**, *128*, 224902.
20. Akcora, P.; *et al.* Anisotropic Self-Assembly of Spherical Polymer-Grafted Nanoparticles. *Nat. Mater.* **2009**, *8*, 354–359.
21. Jain, P. K.; Huang, W.; El-Sayed, M. A. Universal Scaling of Plasmon Coupling in Metal Nanostructures: Extension from Particle Pairs to Nanoshells. *Nano Lett.* **2007**, *7*, 2854–2858.
22. Jain, P. K.; El-Sayed, M. A. Surface Plasmon Coupling and Its Universal Size Scaling in Metal Nanostructures of Complex Geometry: Elongated Particle Pairs and Nanosphere Trimers. *J. Phys. Chem. C* **2008**, *112*, 4954–4960.
23. Wu, M. W.; Register, R. A.; Chaikin, P. M. Shear Alignment of Sphere-Morphology Block Copolymer Thin Films with Viscous Fluid Flow. *Phys. Rev. E* **2006**, *74*, 040801(R).
24. DeRouchey, J.; Thurn-Albrecht, T.; Russell, T. P.; Kolb, R. Block Copolymer Domain Reorientation in an Electric Field: An *In-Situ* Small-Angle X-ray Scattering Study. *Macromolecules* **2004**, *37*, 2538–2543.
25. Olszowka, V.; Hund, M.; Kuntermann, V.; Scherdel, S.; Tsarkova, L.; Böker, A.; Krausch, G. Large Scale Alignment of a Lamellar Block Copolymer Thin Film *via* Electric Fields: A Time-Resolved SFM Study. *Soft Matter* **2006**, *2*, 1089–1094.
26. Sau, T. K.; Murphy, C. J. Seeded High Yield Synthesis of Short Au Nanorods in Aqueous Solution. *Langmuir* **2004**, *20*, 6414–6420.
27. Nikoobakht, B.; El-Sayed, M. A. Preparation and Growth Mechanism of Gold Nanorods (NRs) Using Seed-Mediated Growth Method. *Chem. Mater.* **2003**, *15*, 1957–1962.
28. Pierrat, S.; Zins, I.; Breivogel, A.; Sonnichsen, C. Self-Assembly of Small Gold Colloids with Functionalized Gold Nanorods. *Nano Lett.* **2007**, *7*, 259–263.
29. Landini G. Particles8_Plus for ImageJ, available from http://www.dentistry.bham.ac.uk/landinig/software (accessed on April 8, 2010).